POLITECNICO DI TORINO

Master's Degree in Physics of Complex Systems

Master's Degree Thesis

EFFECTS OF MEMBRANE CURVATURE ON MOLECULAR SORTING

Supervisors

Prof. Luca DALL'ASTA

Prof. Andrea GAMBA

Candidate

Camilla SPRETI

July 2023

Summary

Molecular sorting is the main biological mechanism, which allows eucaryotic cells to organize chemical factors in specific membrane regions, in order to maintain their functions. A recent phenomenological theory has proposed that this process could occur by combining two physical phenomena: molecular self-aggregation and vesicle nucleation. To further investigate molecular sorting, these previous works introduced a minimal lattice-gas model and described the lipid membrane as a two-dimensional flat surface [1, 2]. Here, we develop the model, considering various aspects of molecular sorting on different surfaces, which describe the lipid membrane, in order to analyze the possible effects due to curvature. Based on previous studies [3], our goal is to show that nucleation and domain extraction occur more in regions with high curvature. For this purpose, we study the phenomenon of molecular sorting on three fixed surfaces: a flat surface, with zero curvature, a spherical surface, with constant curvature and an ellipsoidal surface, with variable curvature. Furthermore, we also investigate various properties of nucleation and statistical correlation between domains.
The membrane is simulated with a Gillespie algorithm, used to reproduce phenomena of insertion, diffusion, domain aggregation and extraction.

Table of Contents

List of Figures

Chapter 1

Introduction

Molecular sorting is the main mechanism that regulates the organization of matter in eukaryotic cells. It allows cells to counteract the homogenizing effect of diffusion through sorting and distillation of specific proteins in submicrometric lipid vesicles, which are then detached from the membrane and transported towards appropriate destinations by active mechanisms [4, 5].
Molecular sorting occurs on the plasma membrane, on inner vesicular bodies (endosomes) and in the membrane network of the Golgi apparatus.
Recently a phenomenological theory [1, 2] has proposed that the process could take place by combining two physical phenomena (a) molecular self-aggregation, which induces phase separation, and (b) vesicle nucleation, originating from domain-induced membrane bending.
Studies, concerning the phase nucleation in curved space, have shown that both nucleation and domain growth are strongly affected by the curvature. In particular, critical nuclei form faster on regions with positive Gaussian curvature [3]. Experimentally, it has been demonstrated that protein transport from the endoplasmic reticulum (ER) to the Golgi apparatus occurs in specialized regions, localized on high-curvature ER domains [6].
It has also been observed that the nucleation probability of sorting domains is not spatially homogeneous, but domains cluster into "hotspots" or "nucleation organizers" [7].
Following these previous works, we investigate molecular sorting on surfaces, simulating the lipid membrane, with different curvatures (zero, constant and variable), in order to analyze the dependence on curvature, especially for the processes of nucleation and detachment of domains. Furthermore, we compute the pair correlation between nucleation sites on these surfaces to understand if this is an effect due to curvature.
In order to explore computationally the phenomenological theory of molecular sorting on the membrane, we impose that particles behave according to the Markov

process, already used in [1, 2].
The membrane is discretized through square or hexagonal lattices and to simulate its dynamics a Gillespie-like algorithm with updatable rates is used.

Chapter 2

Self-Organized Molecular Sorting

2.1 Phenomenological Theory

In the proposed model [1, 2], molecules arrive on the membrane, diffuse and aggregate in localized enriched domains, which grow by means of molecule absorption. When the domains reach a characteristic size R_E, they are removed from the membrane with the formation of lipid vesicles.
The domains coexist in a non-equilibrium statistically stationary state with the "gas" of molecules, which diffuse freely, continuously repleted.
This process resembles diffusion-limited aggregation (DLA), with the difference that the presence of the cut-off length R_E prevents the formation of large fractal clusters, which would occur in DLA for long times, and maintains the domains approximately round.
Here, domains of size R larger than a critical size R_C grow irreversibly due to the absorption of single diffusing molecules. Diffusion is the dominant contribution of dynamics as long as the average density $\bar{n}$ of gas molecules is kept low. The absorption of molecules causes the region near the cluster to be depleted. Therefore, the density near the boundary of the domain n_0 is different from the bulk density $\bar{n}$.
When the typical inter-domain distance L is larger than R_E, the difference between bulk density and density near the boundary is approximately $\Delta n \sim \bar{n} - n_0 > 0$ and finite, due to the continuous molecule insertion, contrary to classical nucleation theory, where Δn tends to 0.
The quasi-static density profile of molecules, which diffuse freely near a domain of size R, is determined by solving the Laplace equation with Dirichlet boundary conditions.

2.1.1 Flat Surface

For a flat surface,

$$\begin{cases} D\nabla^2 n(r) & = 0 \\ n(R) & = n_0 \\ n(L) & = \bar{n} \end{cases} \tag{2.1}$$

where D is the diffusion coefficient of the gas bulk, r is the distance from the domain center, R is the domain size and L represents the size of the area, which can be influenced by the domain. We obtain

$$n(r) = n_0 + \Delta n \frac{\ln(r/R)}{\ln(L/R)} \tag{2.2}$$

The inward flux of molecules into the domain, through which the latter grows, is defined as

$$\Phi_R = 2\pi R D \partial_r n(r)\Big|_{r=R} = 2\pi D \frac{\Delta n}{\ln(L/R)} \tag{2.3}$$

From eq. (2.3) we can obtain the dynamic equation for domain growth

$$\dot{R} = \frac{A_0 D \Delta n}{R \ln(L/R)} \tag{2.4}$$

with A_0 the area occupied by a single molecule in the domain.
Assuming that domains are equally distributed on the membrane and that $N(t,R)dR$ is the number of domains per unit area of dimension between R and $R+dR$, the number density $N(t,R)$ satisfies the Smoluchowski equation

$$\frac{\partial N}{\partial t} + \frac{\partial}{\partial R}(\dot{R}N) = -\gamma(R)N, \tag{2.5}$$

where $\gamma(R)$ is the mesoscopic extraction rate, assumed to be negligible for $R < R_E$ and constant $\gamma(R) = \gamma_0$ for $R > R_E$.
A stationary solution of (2.5) is

$$N_{st}(R) = \frac{JR\ln(L/R)}{D\Delta n} \exp\left[-\int_0^R dr \frac{r\ln(L/r)\gamma(r)}{A_0 D \Delta n}\right], \tag{2.6}$$

where the normalization factor J can be determined, imposing that in the stationary regime the incoming flux of molecules per unit area ϕ equals the average flux of molecules absorbed in the domain

$$\phi = \int_{R_C}^{\infty} \Phi_R N_{st}(R) dR \tag{2.7}$$

In the regime $R > R_E$, assuming γ_0 is large enough to suppress the number density $N_{st}(R)$, we obtain $J \sim \phi/R_E^2$. In the regime $R < R_E$, where $\gamma(R)$ is negligible, $N_{st}(R)$ has a universal logarithmic behavior. Assuming that the incoming flux is equally divided among all domains, the average number of domains per unit area is

$$N_d = \int dR N_{st}(R) \sim \frac{\phi}{D\Delta n}. \tag{2.8}$$

The efficiency of the sorting process can be evaluated, considering the average residence time $\bar{T}$ of a molecule on the membrane. This is the sum of the average time $\bar{T}_f$, which the molecule takes to reach the domain by diffusion and be absorbed, and the average time $\bar{T}_d$ spent within the domain.
$\bar{T}_f$ is inversely proportional to the average number of domains per unit area N_d and to the diffusion coefficient D

$$\bar{T}_f \sim \frac{1}{DN_d} \sim \frac{\Delta n}{\phi}, \tag{2.9}$$

while $\bar{T}_d$ can be estimated as

$$\bar{T}_d \sim \frac{R_E^2}{A_0 \Phi_R} \sim \frac{R_E^2}{DA_0 \Delta n}. \tag{2.10}$$

The rate of formation of new domains can be evaluated as

$$\frac{dN}{dt} = CD\bar{n}^2, \tag{2.11}$$

where C is a dimensionless constant, taking into account the efficiency of the absorption of a single molecule. In the stationary state, this rate is given by $N_d/\bar{T}_d$, then

$$\bar{n} \sim \left(\frac{N_d}{CD\bar{T}_d}\right)^{1/2} \sim \left(\frac{\phi A_0}{CDR_E^2}\right)^{1/2} \tag{2.12}$$

Assuming that domains absorb very quickly, causing a very low density in the depleted region near them ($\bar{n} >> n_0$ and $\Delta n \sim \bar{n}$), we obtain

$$\begin{aligned} \bar{T}_f &\sim C^{-1/2} \frac{A_0^{1/2}}{(D\phi)^{1/2} R_E} \\ \bar{T}_d &\sim C^{1/2} \frac{R_E^3}{(D\phi)^{1/2} A_0^{3/2}} \end{aligned} \tag{2.13}$$

Now the average residence time $\bar{T} = \bar{T}_f + \bar{T}_d$ has a minimum, with respect to C, at $C \sim A_0^2/R_E^4$. In the minimum

$$\bar{T}_f \sim \bar{T}_d \sim \frac{R_E}{(DA_0)^{1/2} \phi^{1/2}} \tag{2.14}$$

$$\bar{n} \sim \Delta n \sim \frac{\phi^{1/2} R_E}{(D A_0)^{1/2}} \tag{2.15}$$

These two scaling relations identify the optimal regime, in which molecular sorting is most efficient.
The molecule density inside the domains is expressed as the product of the number of domains per unit area and the number of molecules in a domain

$$\rho_d \sim N_d \frac{R_E^2}{A_0} \sim C^{1/2} \frac{\phi^{1/2} R_E^3}{D^{1/2} A_0^{3/2}} \tag{2.16}$$

Repeating the calculation for the minimum for the total average density $\bar{\rho} = \rho_d + \bar{n}$, we find that this also has a minimum at $C \sim A_0^2/R_E^4$ and in such minimum $\bar{\rho}$ assumes the same value of (2.15).

2.1.2 Curved Surface

For a $(d-1)$-dimensional surface, embedded in a d-dimensional space, any point is specified by a d-dimensional vector $\vec{R}(\vec{x})$, function of the $(d-1)$ coordinates $\vec{x} = (x^1, \ldots, x^{d-1})$.
We can introduce the Monge gauge in order to describe the surface with a single function, the height over a reference plane. In the case of a two-dimensional surface the vector $\vec{R}$ can be written as $\vec{R}(x, y) = (x, y, h(x, y))$, where (x, y) are the coordinates of the point projected onto the reference plane and $h(x, y)$ is the height of the point on the surface.
For the sake of simplicity we consider a spherical surface, with radius of the sphere ρ, and we replace the (x, y) coordinates with r, the distance, projected onto the reference plane, of the point from the center of the domain (Fig. 2.1). In this way $\vec{R} = (r, h(r))$

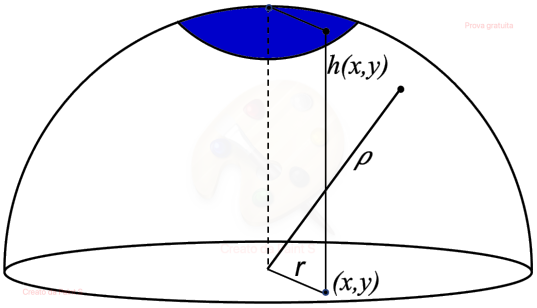

Figure 2.1: Surface described in the Monge gauge. In blue the domain.

In this framework the Laplace equation becomes

$$\begin{cases} \frac{D}{r\sqrt{1+(h'(r))^2}} \frac{\partial}{\partial r} \left(\frac{r}{\sqrt{1+(h'(r))^2}} \frac{\partial n(r)}{\partial r} \right) & = 0 \\ n(R) & = n_0 \\ n(L) & = \bar{n} \end{cases} \tag{2.17}$$

To determine the density profile, we set

$$\frac{r}{\sqrt{1+(h'(r)^2}} \frac{\partial}{\partial r} n(r) = \alpha = cost \tag{2.18}$$

and we integrate

$$\int_R^r dr' \frac{\partial n(r')}{\partial r'} = \alpha \int_R^r dr' \frac{\sqrt{1+(h'(r'))^2}}{r'} \tag{2.19}$$

Introducing the radius of the sphere, representing the curvature, with the change of variables $h(r) = \sqrt{\rho^2 - r^2}$ and solving the integral, we obtain the density profile

$$n(r) = n_0 + \Delta n \frac{\tanh^{-1}\left(\sqrt{\frac{\rho^2-r^2}{\rho^2}}\right)\Big|_r^R}{\tanh^{-1}\left(\sqrt{\frac{\rho^2-r^2}{\rho^2}}\right)\Big|_L^R} \tag{2.20}$$

and the inward flux

$$\Phi_R = 2\pi D \frac{\Delta n}{\tanh^{-1}\left(\sqrt{\frac{\rho^2-r^2}{\rho^2}}\right)\Big|_L^R} \tag{2.21}$$

2.2 Lattice-gas Model

To further explore self-organized molecular sorting, we introduce a lattice-gas model, where each lattice site can host at most one molecule. The system behaves as a Markov process, which is described by the following moves:

- Insertion: molecules arrive on the surface from an infinite reservoir and are inserted on empty sites with rate kI;
- Diffusion: molecules can make a diffusive jump to any empty neighbor with rate $\frac{k_D \cdot n_E}{g^{n_H}}$, with k_D diffusion rate, g aggregation coefficient that accounts for the tendency of molecules to stick together when they meet, n_E the number of empty neighbors and n_H the number of occupied neighbors of the site initially occupied by the jumping molecule;
- Extraction: molecules belonging to the same cluster are extracted by simultaneous removal, if the size of the cluster exceeds the characteristic size R_E.

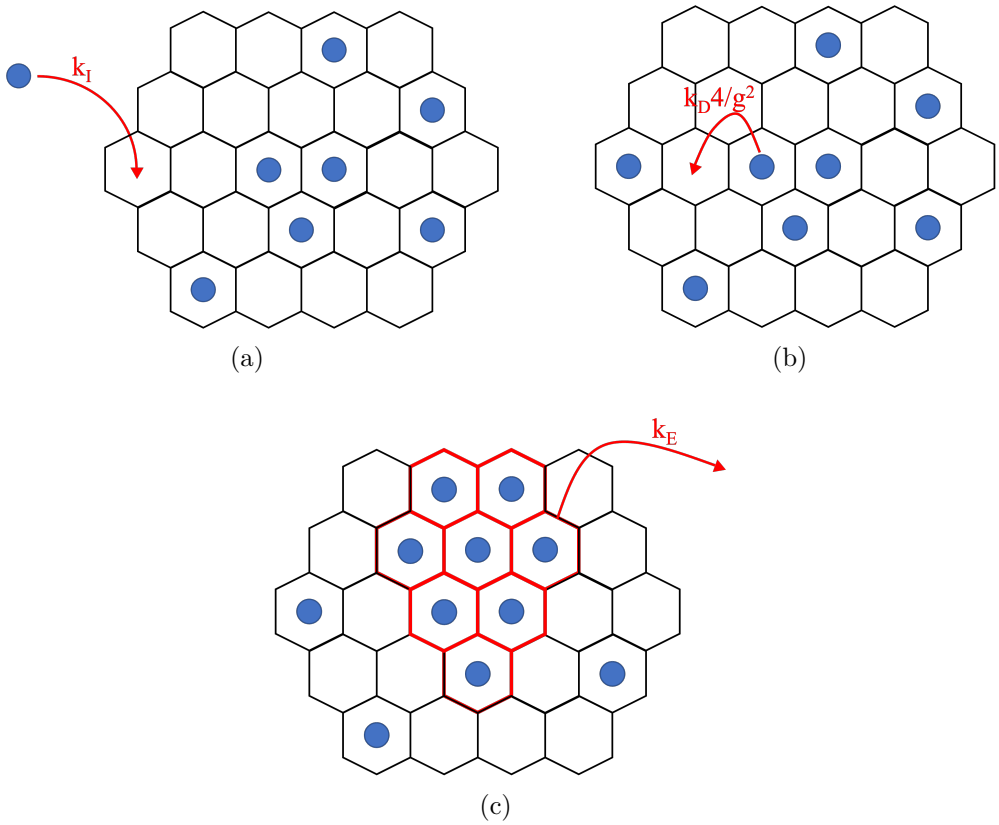

Figure 2.2: Three possible moves of the Markov process: (a) insertion, (b) diffusion, (c) extraction.

2.3 Optimal Sorting

The stationary behavior of the model depends only on two parameters, the ratio k_I/k_D and the aggregation coefficient g. In all numerical simulations the ratio $k_I/k_D = 10^{-6}$, to have a realistic flux entering the membrane. The choice on g is made in order to ensure an optimal sorting regime, corresponding to a minimum of the total stationary density of molecules $\bar{\rho}$.
Figure 2.3 shows that in the case of a hexagonal lattice, for intermediate values of g, the stationary density takes small values and the minimum is in $g = 10$. Instead for a square lattice, the minimum is obtained for $g = 50$.

The efficiency of the sorting process can be estimated by measuring the stationary average molecule density $\bar{\rho}$ on the membrane, since this is proportional to the average residence time $\bar{T}$ of molecules and therefore to the sorting rate $\bar{T}^{-1}$. To demonstrate this, let the average residence time $\bar{T}$ of a molecule on the membrane

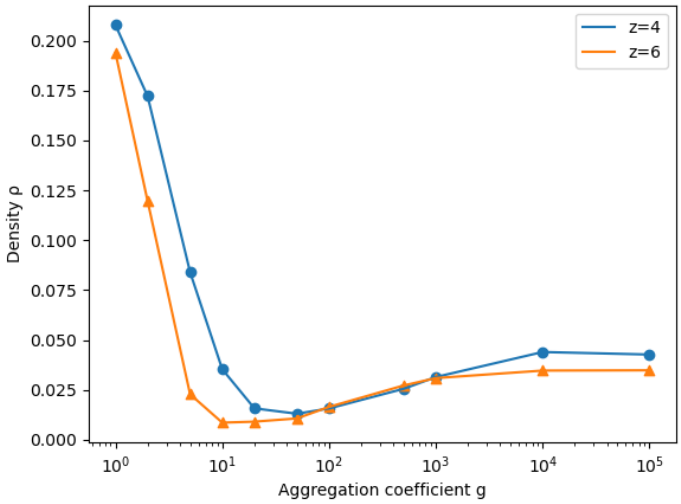

Figure 2.3: Stationary total molecule density ρ as a function of the aggregation coefficient g for different values of the valence z.

be a stochastic variable with probability density $p(t)$. The average density $\bar{\rho}$ of molecules at time t is given by the sum of the ϕdt molecules inserted on average into the system in the previous infinitesimal time intervals dt, where ϕ is the flux of incoming molecules. Adding the condition that the residence time has not yet elapsed, we have

$$\bar{\rho} = \int_0^\infty \text{Prob}(T > t)\phi dt = \phi \int_0^\infty \left(\int_t^\infty p(\tau)d\tau \right) dt = \phi \int_0^\infty \tau p(\tau)d\tau = \phi \bar{T} \quad (2.22)$$

So, the average residence time $\bar{T}$ of a molecule on the membrane is $\bar{T} = \bar{\rho}/\phi$ [1].

Chapter 3

Curvature

The curvature is a geometric concept describing how much an object deviates from being flat. It is defined on each point of the surface and it can be of two types: extrinsic and intrinsic. The extrinsic curvature of an object is measured in relation to a flat space in which the object is immersed. The intrinsic one depends only on the points of the object itself. In our case, where the reference surface is a convex one, we use the Gaussian curvature, which is an intrinsic curvature, defined as the product of the two main curvatures.
Suppose we are given a surface, embedded in the 3-dimensional space and we take a non-singular point (x_0, y_0, z_0) on it. Now we choose an orthonormal frame, where z is normal to the surface while x and y are tangent to it. Then locally near the point (x_0, y_0, z_0) the surface is given in the form $z = f(x, y)$, $z_0 = f(x_0, y_0)$ and

$$\left.\frac{\partial f}{\partial x}\right|_{x_0,y_0} = \left.\frac{\partial f}{\partial y}\right|_{x_0,y_0} = 0 \tag{3.1}$$

Now we construct the Hessian matrix

$$H = \begin{pmatrix} \frac{\partial^2 f}{\partial x^2} & \frac{\partial^2 f}{\partial x \partial y} \\ \frac{\partial^2 f}{\partial y \partial x} & \frac{\partial^2 f}{\partial y^2} \end{pmatrix} \tag{3.2}$$

and we have that the principal curvatures of the surface are the eigenvalues of H at the point where the surface is given in the form $z = f(x, y)$ and $\nabla f = 0$.

Since the Gaussian curvature is the product of the two principal curvatures, we find that it is the determinant of H. [8]

3.1 Calculation of Surface Curvature in Implicit Form

In our work we evaluate the Gaussian curvature, using the implicit formula of the surface. Given the surface as the locus of points where a function in three variables is canceled $F(x, y, z) = 0$, we define

$$\nabla F = \left(\frac{\partial F}{\partial x}, \frac{\partial F}{\partial y}, \frac{\partial F}{\partial z}\right) = (F_x, F_y, F_z) \tag{3.3}$$

$$H(F) = \begin{pmatrix} F_{xx} & F_{xy} & F_{xz} \\ F_{yx} & F_{yy} & F_{yz} \\ F_{zx} & F_{yz} & F_{zz} \end{pmatrix} = \nabla(\nabla F) \tag{3.4}$$

$$H^*(F) = \begin{pmatrix} F_{yy}F_{zz} - F_{yz}F_{zy} & F_{yz}F_{zx} - F_{yx}F_{zz} & F_{yx}F_{zy} - F_{yy}F_{zx} \\ F_{xz}F_{zy} - F_{xy}F_{zz} & F_{xx}F_{zz} - F_{xz}F_{zx} & F_{xy}F_{zx} - F_{xx}F_{zy} \\ F_{xy}F_{yz} - F_{xz}F_{yy} & F_{yx}F_{xz} - F_{xx}F_{yz} & F_{xx}F_{yy} - F_{xy}F_{yx} \end{pmatrix} \tag{3.5}$$

The Gaussian curvature is defined, at each point where $\nabla F \neq 0$, as

$$G = \frac{\nabla F H^*(F) \nabla F^T}{||\nabla F||^4} \tag{3.6}$$

3.1.1 The Case of Ellipsoid

The ellipsoid is the locus of points such that $F(x, y, z) = \frac{x^2}{a^2} + \frac{y^2}{b^2} + \frac{z^2}{c^2} - 1 = 0$. The gradient is

$$\nabla F = \left(\frac{2x}{a^2}, \frac{2y}{b^2}, \frac{2z}{c^2}\right) \tag{3.7}$$

and the Hessian is

$$H(F) = \begin{pmatrix} \frac{2}{a^2} & 0 & 0 \\ 0 & \frac{2}{b^2} & 0 \\ 0 & 0 & \frac{2}{c^2} \end{pmatrix}, \tag{3.8}$$

from which

$$H^*(F) = \begin{pmatrix} \frac{4}{b^2c^2} & 0 & 0 \\ 0 & \frac{4}{a^2c^2} & 0 \\ 0 & 0 & \frac{4}{a^2b^2} \end{pmatrix}. \tag{3.9}$$

We can therefore compute the Gaussian curvature

$$G = \frac{\left(\frac{2x}{a^2}, \frac{2y}{b^2}, \frac{2z}{c^2}\right) \begin{pmatrix} \frac{4}{b^2c^2} & 0 & 0 \\ 0 & \frac{4}{a^2c^2} & 0 \\ 0 & 0 & \frac{4}{a^2b^2} \end{pmatrix} \begin{pmatrix} \frac{2x}{a^2} \\ \frac{2y}{b^2} \\ \frac{2z}{c^2} \end{pmatrix}}{\left(\frac{4x^2}{a^4} + \frac{4y^2}{b^4} + \frac{4z^2}{c^4}\right)^2} \tag{3.10}$$

3.1.2 The Case of the Sphere

The sphere is the locus of points such that $F(x, y, z) = x^2 + y^2 + z^2 - R^2 = 0$. The gradient is

$$\nabla F = (2x,2y,2z) \tag{3.11}$$

and the Hessian is

$$H(F) = \begin{pmatrix} 2 & 0 & 0 \\ 0 & 2 & 0 \\ 0 & 0 & 2 \end{pmatrix}, \tag{3.12}$$

from which we obtain

$$H^*(F) = \begin{pmatrix} 4 & 0 & 0 \\ 0 & 4 & 0 \\ 0 & 0 & 4 \end{pmatrix}. \tag{3.13}$$

Then, the Gaussian curvature is

$$G = \frac{(2x, 2y, 2z) \begin{pmatrix} 4 & 0 & 0 \\ 0 & 4 & 0 \\ 0 & 0 & 4 \end{pmatrix} \begin{pmatrix} 2x \\ 2y \\ 2z \end{pmatrix}}{(4x^2 + 4y^2 + 4z^2)^2} = \tag{3.14}$$

$$= \frac{16(x^2 + y^2 + z^2)}{16(x^2 + y^2 + z^2)^2} = \frac{1}{R^2}$$

Curvature formulas for implicit surfaces are taken from [9].

Chapter 4

Simulation methods

4.1 Lattice Construction

The lattice on the ellipsoidal and spherical surface, used to discretize the membrane, is generated in Matlab, using a triangular mesh generator [10]. Then the dual hexagonal lattice is built. Since it is not possible to cover the surface with only hexagons, there are some defects, such as pentagons and heptagons, on which corrections must be applied.

4.2 Model Implementation

To simulate the dynamics on the lipid membrane, we implement a Gillespie-like algorithm, using the CavityTools library [11]. In particular, we use the ExponentialQueue library to sample events in continuous time. We construct an updatable queue of $2N + 1$ events, where the first N rates are associated with diffusive events, the second N are associated with insertion events and the last one is the extraction rate; then at each time step a rate, deciding the type of move, is selected. Both the queue and various quantities, calculated initially and describing the arrangement of molecules, are updated during the dynamics.

For the complete code see https://github.com/Camilla9802/Molecular-sorting-on-a-curved-membrane.git.

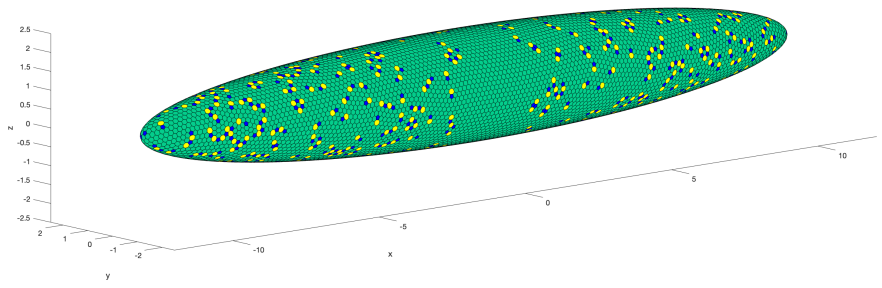

(a)

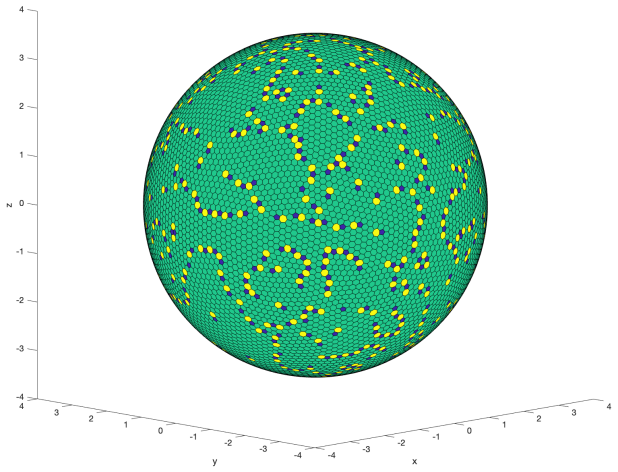

(b)

Figure 4.1: Lattice on (a) ellipsoidal and (b) spherical surfaces: pentagons (blue), hexagons (green), heptagons (yellow)

Chapter 5

Diffusion and Extraction processes

5.1 Correction of Defects

Without applying modifications to correct defects, seen in Chapter 4, the processes of insertion, diffusion, aggregation and extraction have strong inhomogeneities, caused by the different number of neighbors for the three types of polygons. Indeed in all mechanisms on average, the heptagons are sampled more than the hexagons and the pentagons less. In the case of aggregation and extraction, the heptagons occupied by a molecule, having more neighbors, are more likely to attract other molecules, form clusters and therefore be extracted (Fig. 5.1). For the same reason in the diffusive jump an empty heptagon is more likely to be selected as the arrival site.
In order to balance these mechanisms we correct diffusion and aggregation coefficients, introducing effective coefficients for each site:

$$\begin{aligned} k_{D,i}^{eff} &= k_D \cdot \frac{\overline{n}}{n_i} \\ g_i^{eff} &= g^{\frac{\overline{n}}{n_i}} \end{aligned} \tag{5.1}$$

for $i = 1, \ldots, N$ and where $\overline{n}$ is the average number of neighbors in the lattice (in our case $\overline{n} = 6$) and n_i is the number of neighbors of the i-th site. In this way the process provides the equilibrium distribution. To make it uniform we implement a Metropolis-Hastings algorithm: in the diffusive jump, once randomly selected the arrival site, we accept the move with probability p and reject it with probability $1 - p$, where $p = \frac{\text{neighbors of the source site}}{\text{neighbors of the selected site}}$.

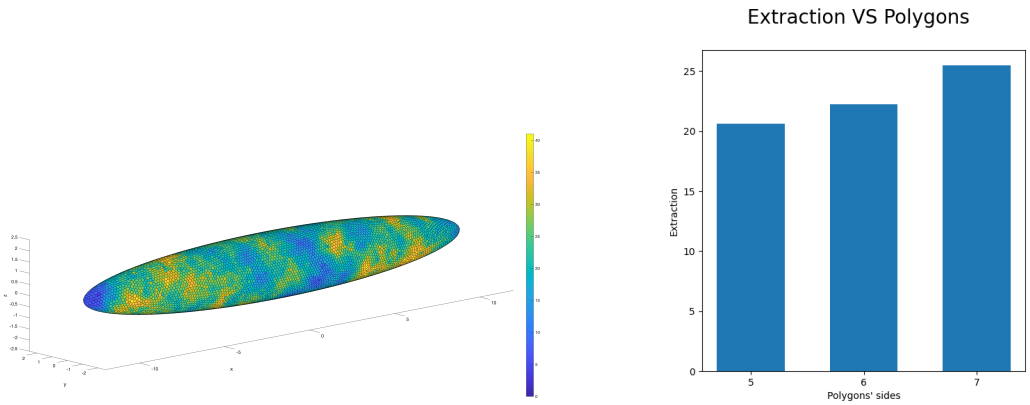

(a) (b)

Figure 5.1: (a) Number of times a molecule is extracted from the site. Regions with more extractions are concentrated around the heptagons, showing how the model without corrections depends on the topology of the lattice. (b) Histogram of the average number of extractions according to the type of polygon.

We can observe that with the corrections introduced previously both the diffusion and the extraction are balanced with respect to the number of neighbors (Fig. 5.2). In addition, the diffusion process is homogeneous throughout the lattice 5.3(a).

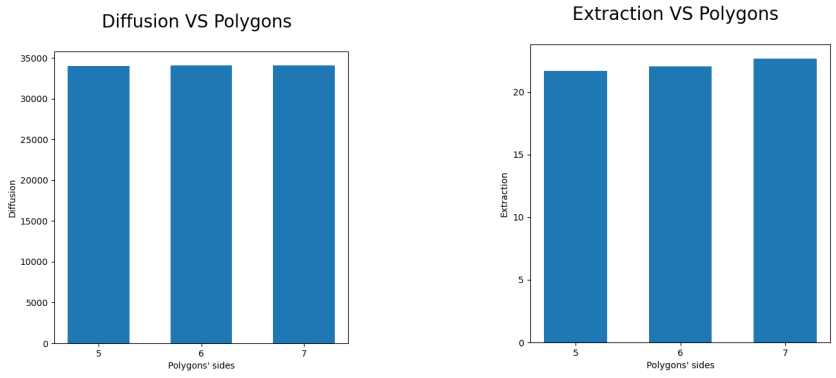

(a) (b)

Figure 5.2: (a) Histogram of the average residence time as a function of the type of polygon in the diffusive process. (b) Histogram of the average number of extractions according to the type of polygon.

In the extraction mechanism, however, despite the corrections, we continue to see

regions where extraction events occur more frequently (Fig. 5.3(b)). Now we need

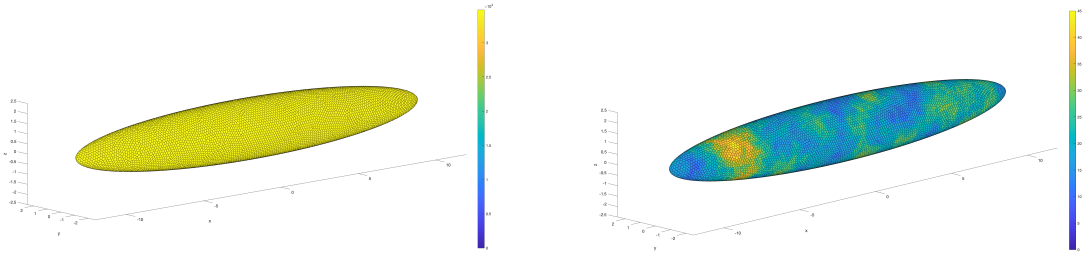

(a) (b)

Figure 5.3: (a) Residence time of the molecules on the sites in the diffusive process. (b) Number of extractions per site.

to understand if the formation of these regions is due to the curvature of the surface or to some correlation between clusters, which we have not yet considered.

5.2 Study of Different Surfaces

In order to understand if the phenomenon described above is an effect of curvature, we perform the same simulations on the spherical surface, which has constant curvature, and on the flat square lattice, which has zero curvature. We expect that, if so, in both cases the formation of these regions, favored in the extraction of clusters, should not be observed. In addition, in the case of the flat surface, using a regular square lattice, we also remove the possible residual effects due to defects, so we expect to observe an even more homogeneous phenomenon. Contrary to the expected results, we observe how the hotspots are also present on these structures (Fig. 5.4).

5.3 Averages over Multiple Simulations

Assuming that the formation of these hotspots may be due to a memory internal to the process, we perform a statistical average over several simulations with different initial conditions. By averaging multiple simulations on the flat lattice, we obtain a sufficiently homogeneous extraction process. From Figure 5.5(a) we see how the difference in the number of extractions per site on the flat lattice has decreased compared to what is observed in Figure 5.4(b). On the curved surface, however, although this difference has decreased compared to Figure 5.3(b), it continues to be not negligible. In particular, we observe the formation of two "strips" of sites

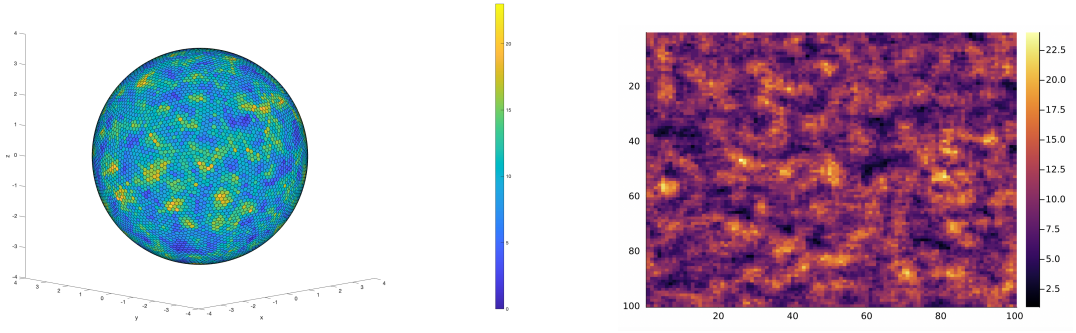

(a) (b)

Figure 5.4: Number of extractions per site (a) on the spherical surface and (b) on the flat surface.

most sampled in areas with intermediate curvature 5.5(b). This fact is further highlighted, by computing averages, no longer total, but on "slices" of the surface. We divide the ellipsoidal surface into spherical crowns along the x-axis and measure the statistical average for each crown (Fig. 5.6).

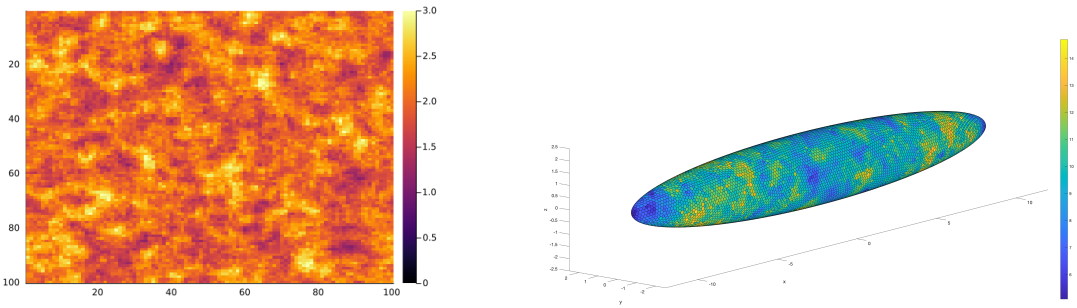

(a) (b)

Figure 5.5: Average number of times a molecule is extracted from the site: (a) on a flat lattice over 20 simulations; (b) on a curved surface over 10 simulations.

We assume, therefore, that a trapping phenomenon occurs in these areas. The idea is as follows: in these intermediate regions, since there is less physical space, freely diffusing molecules, described as hard spheres that cannot overlap, are more likely to encounter other molecules and stick together, forming clusters. New particles, arriving in these areas, are attracted, through the aggregation force g, towards these clusters and remain trapped. With this mechanism, these domains reach the extraction size faster and this would explain the increased extraction activity on

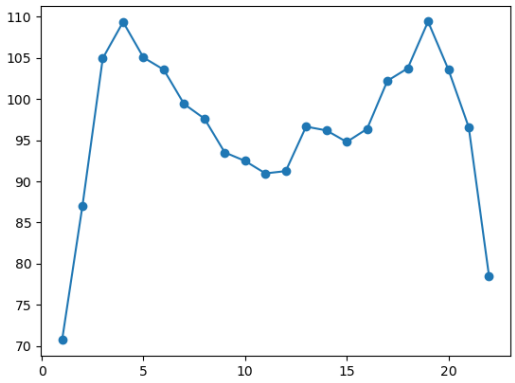

Figure 5.6: Average number of extraction on each spherical crown

these stripes.

Chapter 6

Nucleation and Domain Growth

The phenomenon of nucleation is the mechanism through which the phase transition can occur. Once the core is formed, starting the phase change, it grows until the phase transition has taken place completely.

By studying nucleation and growth phenomena (NG) on substrates with curvature, it has been observed that the curved geometry itself makes the phenomenon non-homogeneous [3]. Considering spherical substrates, i.e. with positive Gaussian curvature, it has been shown that for geometric reasons (compared with the plane, for a given perimeter a circle has more area on the spherical curvature) the critical size of the domains decreases when decreasing the radius of the sphere, meaning that NG is favored for higher curvatures. This implies that for higher positive curvatures the growth of the nuclei is faster.

Now we perform nucleation and cluster growth experiments on our cigar-like surface, shown above (Fig. 4.1). We proceed by seeding an almost circular nucleus of a predefined initial size both on the region with higher curvature (the pole), and on the almost flat region and we study its temporal evolution.
We observe that on average the nuclei, located on the pole, reach the maximum size faster than those placed on the flat region, but the latter reach much larger dimensions (Fig. 6.1).
This effect may be due to two different phenomena. First, on the flat region, molecules have more physical space to move, so they have more paths to attach to the cluster. On the other hand, it has been shown that diffusivity is strongly affected by the geometry of the surface [12]. Precisely, the diffusion coefficient decreases as the curvature increases, which means that particles diffuse more slowly

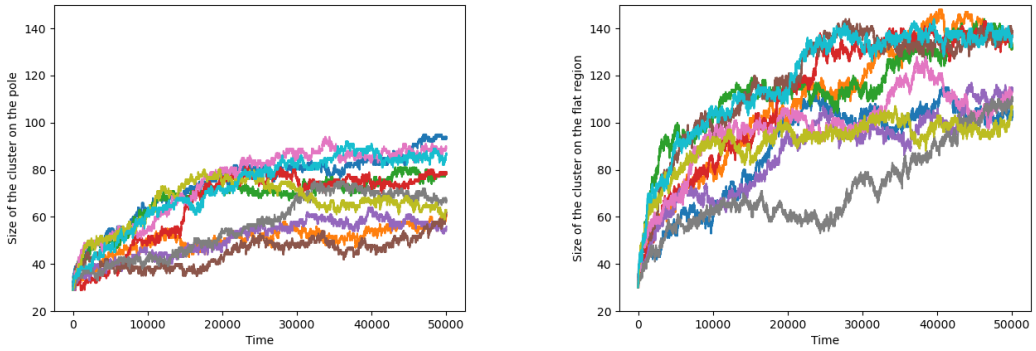

(a) (b)

Figure 6.1: Temporal evolution of the cluster (a) on the pole and (b) on the flat region over 10 simulations.

in high-curvature areas and take longer to reach the pole. As a result, we have clusters on the poles that grow less, but are more stable, because particles arriving on the pole are trapped due to low diffusivity.
Furthermore, we analyze the secondary domains that are formed during the diffusion process. From Figure 6.2 we see that when the initial cluster is seeded on the pole, during the dynamics on average at least another domain is formed, which nucleates far from the first one. Otherwise, if the initial cluster is placed on the flat region, more frequently we observe situations with the initial domain only. In this case, the secondary clusters organize independently of the first. This seems to validate what was said above.

To investigate the phenomenon further, we replicate the experiments on an ellipsoidal surface, where the difference in curvature is smaller. Here, as we expected, both cases appear more balanced, meaning that the behaviors seen before are related to the curvature of the membrane (Fig. 6.3).

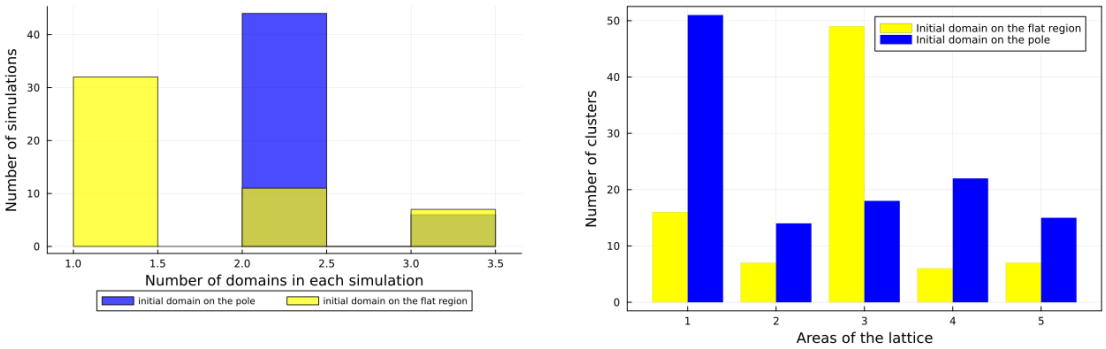

(a) (b)

Figure 6.2: (a) Number of clusters and (b) positions of secondary clusters, over 50 simulations. We divided the x-axis into 5 sectors, such that each sector contains the same number of sites, and counted the domains within each intervals. The two highest bars represent the initial nuclei on the pole and on the flat region, respectively.

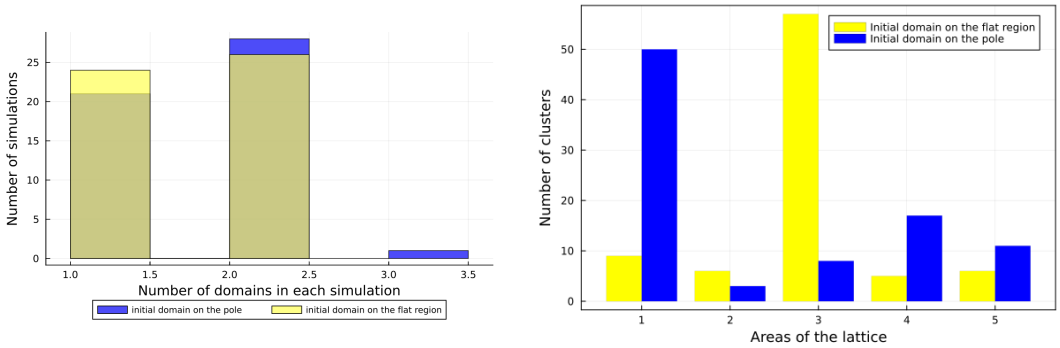

(a) (b)

Figure 6.3: (a) Number of clusters and (b) positions of secondary clusters, over 50 simulations. We divided the x-axis into 5 sectors, such that each sector contains the same number of sites, and counted the domains within each intervals. The two highest bars represent the initial nuclei on the pole and on the flat region, respectively.

Chapter 7

Correlation Analysis

After having found that the appearance of hotspots does not depend on the curvature of the membrane, we carry out a detailed study of the correlation between domains. In a study of clathrin-mediated endocytosis, it was experimentally demonstrated that clathrin-coated pits at the plasma membrane repeatedly form at predefined sites [7]. To assay the spatial distribution of nucleation sites, the pair correlation function, derived from Ripley's K-function, was used. It has been shown that for small distances the pair correlation function takes values > 1, meaning that nucleation sites tend to cluster. Instead, for a spatially random distribution, the function has a constant value equal to the average density of points, with which it is then normalized (Fig. 7.1).

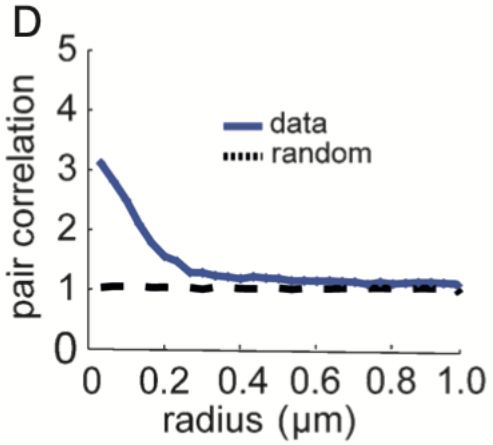

Figure 7.1: Pair correlation function of all nucleation events, captured by the detection (blue) and pair correlation function of a random distribution [7].

7.1 Pair Correlation

Here we replicate the same quantitative analysis of spatial clustering, through Ripley's K-function [13].

7.1.1 Empirical K-function

The empirical K-function is the cumulative average number of data points, lying within a distance r, corrected for edge effects:

$$\hat{K}(r) = \frac{|W|}{n(n-1)} \sum_{i=1}^{n} \sum_{j \neq i, j=1}^{n} \mathbf{1}\{d_{ij} < r\} e_{ij}(r) \tag{7.1}$$

where n is the number of points, $|W|$ is the area of the observation window, d_{ij} is the distance between point i and point j and e_{ij} is an edge correction weight, necessary to account for the missing observations for points located at the edge of the image, which may have additional 'invisible' close neighbor points located outside of the image.

7.1.2 Empirical Pair Correlation Function

The pair correlation function $g(r)$ in two dimensions is defined as

$$g(r) = \frac{K'(r)}{2\pi r} \tag{7.2}$$

where $K'(r)$ is the derivative of K with respect to r.
To estimate the pair correlation function we employ the kernel smoothing technique: we replace the indicator function $\mathbf{1}\{d_{ij} < r\}$ with a kernel term $\kappa(d_{ij} - r)$

$$\hat{g}(r) = \frac{|W|}{2\pi r n(n-1)} \sum_{i=1}^{n} \sum_{j \neq i, j=1}^{n} \kappa_h(r - d_{ij}) e_{ij}(r) \tag{7.3}$$

where the smoothing kernel κ_h, with smoothing bandwidth $h > 0$, is a rescaled kernel term

$$\kappa_h(x) = \frac{1}{h} \kappa\left(\frac{x}{h}\right) \tag{7.4}$$

For example, κ could be the standard normal density function

$$\kappa(x) = \frac{e^{-x^2/2}}{\sqrt{2\pi}} \Rightarrow \kappa\left(\frac{x}{h}\right) = \frac{e^{-x^2/2h^2}}{\sqrt{2\pi}}, \tag{7.5}$$

so that κ_h would be the normal density function with 0 mean and standard deviation h

$$\kappa_h(x) = \frac{e^{-x^2/2h^2}}{h\sqrt{2\pi}} \tag{7.6}$$

7.1.3 Edge Correction

Regarding the edge correction weight, we introduce a correction factor

$$c(d_e, r) = \begin{cases} \frac{\pi + 2\sin^{-1}(d_e/r)}{2\pi} & \text{for } r > d_e \\ 1 & \text{otherwise} \end{cases} \tag{7.7}$$

where d_e denotes the distance between point i and the nearest boundary [14].

7.1.4 Correlation through Simulations

We numerically replicate the procedure, shown above, to measure the pair correlation function between domains of size = 20 sites occupied on a 100x100 flat lattice.

Unlike biological results, we do not find the presence of a spatial correlation between domains, which seem to be randomly distributed on the lattice (Fig. 7.2).

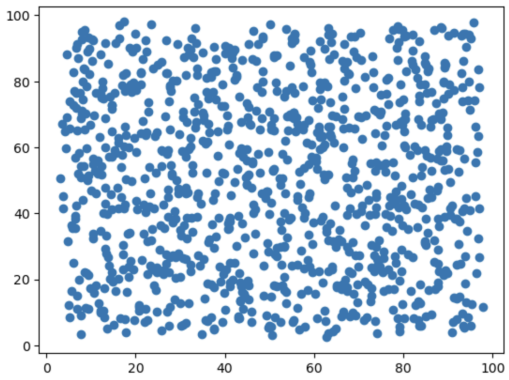

Figure 7.2: Centers of 1000 domains on the flat lattice

7.2 Correlation between Extracted Clusters

Now we study the correlation between domains removed from the membrane. In particular, we consider domains extracted consecutively and we measure pair distances, distinguishing domains formed before the previous extraction and domains formed later. From Figure 7.3, we observe that on average domains formed before tend to localize at greater distances, probably indicating the presence of a repulsive interaction potential between domains. On the contrary, domains formed later are located near the region, left empty by the extracted cluster.

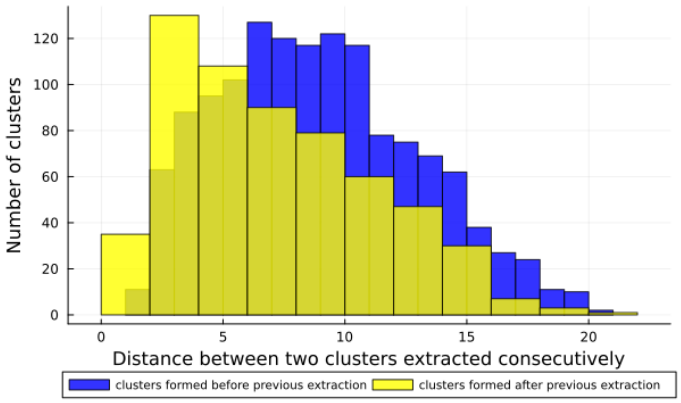

Figure 7.3: Pair distances between clusters extracted consecutively

In our case, we observe only spatial correlations for small times, as shown in Figure 7.3, which are probably averaged over a long time.

Chapter 8

Conclusions

In this work we have studied molecular sorting on geometries with different curvatures, analyzing the effect of the latter on the process.
In the first chapters (2, 3) we have discussed the phenomenological model describing molecular sorting and geometric concepts related to curvature. After illustrating the methods implemented to simulate membrane dynamics (Chapter 4), we have analyzed the diffusion and extraction processes (Chapter 5), and nucleation and growth of domains (Chapter 6) on our reference surfaces. In the last chapter (7), based on biological results, obtained from the study of clathrin, we have measured the spatial correlation between domains.

Exploring various aspects of the mechanisms mentioned above, we have found that diffusion is the governing process in the system. Indeed, we have observed that diffusion is slower with increasing curvature, thus making the sorting process on high-curvature regions more difficult and producing hotspots on regions with intermediate curvature. On the other hand, this low diffusivity at the poles causes the domains, once able to form, to remain trapped, resulting more stable.

Bibliography

[1] Marco Zamparo, Donatella Valdembri, Guido Serini, Igor V Kolokolov, Vladimir V Lebedev, Luca Dall'Asta, and Andrea Gamba. «Optimality in self-organized molecular sorting». In: *Physical Review Letters* 126.8 (2021), p. 088101 (cit. on pp. ii, 1–3, 9).

[2] Elisa Floris, Andrea Piras, Francesco Saverio Pezzicoli, Marco Zamparo, Luca Dall'Asta, and Andrea Gamba. «Phase separation and critical size in molecular sorting». In: *Physical Review E* 106.4 (2022), p. 044412 (cit. on pp. ii, 1–3).

[3] Leopoldo R Gómez, Nicolás A Garcıa, Vincenzo Vitelli, José Lorenzana, and Daniel A Vega. «Phase nucleation in curved space». In: *Nature communications* 6.1 (2015), p. 6856 (cit. on pp. ii, 1, 20).

[4] Ira Mellman and W James Nelson. «Coordinated protein sorting, targeting and distribution in polarized cells». In: *Nature reviews Molecular cell biology* 9.11 (2008), pp. 833–845 (cit. on p. 1).

[5] Sara Sigismund, Stefano Confalonieri, Andrea Ciliberto, Simona Polo, Giorgio Scita, and Pier Paolo Di Fiore. «Endocytosis and signaling: cell logistics shape the eukaryotic cell plan». In: *Physiological reviews* 92.1 (2012), pp. 273–366 (cit. on p. 1).

[6] Michiyo Okamoto, Kazuo Kurokawa, Kumi Matsuura-Tokita, Chieko Saito, Ryogo Hirata, and Akihiko Nakano. «High-curvature domains of the ER are important for the organization of ER exit sites in Saccharomyces cerevisiae». In: *Journal of cell science* 125.14 (2012), pp. 3412–3420 (cit. on p. 1).

[7] Daniel Nunez, Costin Antonescu, Marcel Mettlen, Allen Liu, Sandra L Schmid, Dinah Loerke, and Gaudenz Danuser. «Hotspots organize clathrin-mediated endocytosis by efficient recruitment and retention of nucleating resources». In: *Traffic* 12.12 (2011), pp. 1868–1878 (cit. on pp. 1, 23).

[8] S. P. Novikov and A. T. Fomenko. *Basic Elements of Differential Geometry and Topology*. Vol. 60. Mathematics and its Applications (Soviet series). Kluwer Academic Publishers, 1990 (cit. on p. 10).

[9] Ron Goldman. «Curvature formulas for implicit curves and surfaces». In: *Computer Aided Geometric Design* 22.7 (2005), pp. 632–658 (cit. on p. 12).

[10] Per-Olof Persson and Gilbert Strang. «A Simple Mesh Generator in MATLAB». In: *SIAM review* 46.2 (2004) (cit. on p. 13).

[11] Braunstein Alfredo et al. *CavityTools.jl*. 2023. URL: `https://github.com/abraunst/CavityTools.jl.git` (cit. on p. 13).

[12] Ali Naji and Frank LH Brown. «Diffusion on ruffled membrane surfaces». In: *The Journal of chemical physics* 126.23 (2007) (cit. on p. 20).

[13] A. Baddeley, E. Rubak, and R. Turner. *Spatial Point Patterns: Methodology and Applications with R*. London: Chapman and Hall/CRC, Dec. 2015, pp. 199–254. URL: `http://www.crcpress.com/books/details/9781482210200/` (cit. on p. 24).

[14] Peter Haase. «Spatial pattern analysis in ecology based on Ripley's K-function: Introduction and methods of edge correction». In: *Journal of vegetation science* 6.4 (1995), pp. 575–582 (cit. on p. 25).